Kingdom of Saudi Arabia
Imam Mohammed Ibn Saud
Islamic University
College of Science
Chemistry department

بسم الله الرحمن الرحيم

المملكة العربية السعودية
جامعة الإمام محمد بن سعود الإسلامية
كلية العلوم
قسم الكيمياء

Synthesis of $SrNiO_3$/g-C_3N_4 nanocomposite for efficient removal of organic dyes from wasted water

A graduation research project

Submitted to

Chemistry Department in Partial Fulfillment of the Requirements for the Completion of the Degree of Bachelor of Science in Chemistry

By

Muhannad Khalid Muhammad Al-Dabasi **ID:441017230**

Nawaf Ibrahim Abdullah Al-Muwaizri **ID: 441022159**

Under supervision

By

Prof. Dr. Mohamed Khairy Abdel Fattah

Second Semester, Fab 2025

Acknowledgement

I wish to express my indebtedness and deepest sincere gratitude and appreciation Prof. Dr. Mohamed Khairy AbdelFattah Omran, Prof. of physical chemistry, College of science, Imam Mohammed Ibn Saud Islamic University for his supervision, suggesting the research problem, useful guidance, fruitful discussion encouragement and facilities he offered me throughout the progress of this work.

We also owe a debt of gratitude to the department leader, Dr. Faical. Our path has been greatly aided by his unwavering encouragement and support, but more significantly, by his vision and leadership in fostering an atmosphere that is favorable to research and innovation.

We also want to express our gratitude to the teachers of Al-Imam Mohammad Ibn Saud Islamic University and the academics in our chemistry department for their commitment, instruction, and assistance. Our academic development has benefited greatly from their advice and experience.

Lastly, we express our gratitude to our families for their constant love, support, and encouragement. Throughout this journey, their unwavering believe in us and support have been crucial.

الملخص

نظرا لخطورة تلوث المياه على صحة الانسان لذا من الضروري الاهتمام بتنقية المياه من بعض الملوثات مثل الاصباغ العضوية الناتجة من عدة مصادر مثل صناعة الأصباغ. لذلك يهدف هذا المشروع الي إزالة صبغة النيلى كارمين الزرقاء من المياه باستخدام مواد نانومتريه مكونة من تراكيب من نتريد الكربون الجرافيتي (g-C_3N_4, NiO, $SrNiO_3$. تم تحضير المواد باستخدام طريقة الصول. تم توصيف العينات من خلال عدة أجهزة مثل مطياف الأشعة تحت الحمراء وحيود الأشعة السينية (XRD) وجهاز امتصاص الاشعة فوق البنفسجية والمرئية والميكروسكوب الإلكتروني النافذ. أظهرت النتائج امتصاص التراكيب$SrNiO_3/g-C_3N_4$ للضوء المرئي مما يؤهله ليكون عامل حافز ضوئي نشط. تم فحص التحلل الضوئي لصبغة نيلي كارمين. أظهر التراكيب النانوية $SrNiO_3/g-C_3N_4$ أعلى نشاط تحفيزي ضوئي حيث تم إزالة 100% من الصبغة خلال ساعة.

Abstract

Given the seriousness of water pollution on human health, it is necessary to pay attention to purifying water from some pollutants such as organic dyes resulting from several sources such as the dye industry. Therefore, this project aims to remove indigo carmine blue dye from water using nanomaterials consisting of graphitic carbon nitride (g-C_3N_4) and $SrNiO_3$. The materials were prepared using the sol-gel method. The samples were characterized by several tools such as infrared spectroscopy, X-ray diffraction (XRD), ultraviolet and visible absorption spectrophotometer, and transmission electron microscopy. The results showed that the $SrNiO_3$/g-C_3N_4 nanocomposite absorb visible light, which qualifies them to be an active photocatalyst. The photodegradation of indigo carmine dye was examined. The $SrNiO_3$/g-C_3N_4 nanocomposite showed the highest photocatalytic activity, as 100% of the dye was removed within an hour.

Chapter 1: Introduction

1. Introduction:

1.1. General introduction

Finding creative ways to address the problems of pollution and wastewater treatment is still crucial as materials science and environmental preservation continue to advance. Numerous investigations have been carried out on the application of earth-rich metal oxides as photocatalysts and for the purification of water waste. Because of their low cost and high activity, earth-abundant metal oxides have the potential to be photocatalysts [1–4].

1.2. Water pollution

The presence of any physical, chemical, or biological (biological) compounds in water in excessive amounts that could alter its quality and endanger living things is known as water pollution. Polluted water has an unpleasant taste, but unpolluted water is colorless, odorless, and tasteless. Even while it contains certain invisible contaminants, such insecticides and disease-causing microbes that spread through water, it has an unpleasant odor and can appear hazy and foggy. It is not advisable to drink, farm, bathe, or wash with polluted water. Because contaminants found in water can have varying detrimental effects on human health based on their type and concentration.

1.3. Water treatment methods

The wasted water can be easily treated to remove the pollutants vis several methods such as

1.3.1. Deposition process

It is one of the gravity-based water treatment techniques. This is accomplished by keeping the water motionless and tranquil until high-density particles—which are denser than water—gradually sink to the bottom of the tank or basin. We refer to this process as normal sedimentation.

1.3.2. The process of coagulation or coagulation

To gather suspended materials in which the sedimentation process is unable to remove very fine particles because heavy and massive particles sink to the bottom quickly whereas finer particles take a very long time to settle and often never do [5].

They must therefore come before them. The sedimentation process is a chemical process called coagulation, which involves the addition of chemicals to water to form larger masses of solids from immature particles [5].

1.3.3. Filtering and filtration process

The process that comes after the coagulation process is called the filtration process, and it is a physical procedure that involves spraying water down and passing it through a layer of granular porous materials, like sand, to remove impurities. This traps the suspended particles inside the pores of the filtration media. Additionally, it eliminates dangerous natural colors and protozoa [5].

1.3.4. Photocatalysis and photocatalysts

The words "photo" (from the word "photon") and "catalyst," which refers to a material that changes the rate of a reaction when it is present, are combined to form the term "photocatalyst." Consequently, substances that alter a chemical reaction's pace upon exposure to light are known as photocatalysts. We call this process photocatalysis. Reactions that use a semiconductor and light are referred to as photocatalysis. A photocatalyst is a substrate that both absorbs light and catalyzes chemical reactions. In essence, all photocatalysts are semiconductors. A phenomenon known as photocatalysis occurs when a semiconducting substance is exposed to light, creating an electron-hole pair.

Based on how the reactants' physical states appear, photocatalytic reactions can be divided into two categories.

• *Homogeneous photocatalysis*: Homogeneous photocatalysis is the term used to describe photocatalytic reactions in which the semiconductor and reactant are in the same phase, such as a gas, solid, or liquid.

• *Heterogeneous photocatalysis*: Heterogeneous photocatalysis is the term used to describe photocatalytic reactions in which the reactant and semiconductor are in distinct stages.

1.4. Nanomaterials

Any substance with a composition based on nanoparticle units, such as silver nanoparticles, carbon nanotubes, inorganic ceramic materials, etc., is referred to as a nanomaterial.

Among the many characteristics of nanostructured materials are:

a) Chemical and Surface Activity: The catalytic activity of supported gold catalysts can be increased when the Au particle size is decreased to 2–10 nm.

b) Mechanical: measurements have shown that the hardness of silicon nanospheres (20–50 nm) is four times higher than that of bulk silicon (50 Gpa vs. 12 Gpa). Copper nanoparticles are known to be extremely hard when their size decreases, even if bulk copper is bent.

c) Electronic: Quantum size effects in the confinement affect characteristics like electrical conductivity. Silicon: Conductor to Insulator

d) Magnetic: The magnetic characteristics of transition metal nanoparticles, like Co and Ni, exhibit significant size-dependent changes.

e) Optical: When evenly distributed, nanoparticles that are smaller than the wavelength of light (400–700 nm) look transparent. Copper, for example, is opaque to transparent.

1.5. $SrNiO_3$

The ABO_3 perovskites belong to a class of mixed oxides with the general formula ABO_3, in which B is an ion of a transition metal and A is an ion of lanthanide and/or alkaline earth metal [6]. ABO_3's A and B sites can also hold cations with different charges, creating a spectrum of AB combinations with completely different properties. Combinations like $A^{2+}B^{4+}O_3$, $A^{3+}B^{3+}O_3$, $A^{4+}B^{2+}O_3$, $A^{5+}B^{+}O_3$, and $A^{+}B^{5+}O_3$ can be made with different levels of stability [9]. Most metals from the periodic table can frequently be accommodated in the A or B sites of ABO3 perovskites, resulting in materials with adjustable photocatalytic properties. Solar cells, light-emitting diodes, photodetectors, lasers, and photocatalysts are among the many composites that incorporate perovskite materials [7–10].

In a perovskite structure, the oxygen at the X-site increases the reactivity of the lattice oxygen, the metals at the A-site enhance the material's thermal stability, and the B-site increases catalytic activity [11]. Perovskites allow partial substitution

of cations at A-site and B-site and have an amazing capacity to hold numerous cations. The production of oxygen vacancies and the varying valence state of A- or B-site cations are caused by partial substitution. By examining the adsorption behavior of the reaction intermediate, these modifications and the electrochemical stability in perovskite oxides improve catalytic activity [12]. B-type metals' oxidation and spin states are linked to their energy band gap orbital (Eg) occupancy [13].

1.6. Graphitic carbon nitride (g-C_3N_4)

The semiconductor graphitic carbon nitride is metal-free and possesses a variety of optical, electrical, and catalytic characteristics. Additionally, it has excellent chemical and thermal stability. g-C3N4 can be produced, and it has the ability to gather light sufficiently. in the optical range as nanostructured scaffolds and light-harvesting antennas. It is also more likely to produce doped or heterojunction compounds since g-C3N4 has the narrowest band gap of any g-C3N4 compound. [14].

High N:C ratios are found in carbon nitrides. Their structures range from polymeric to graphitic. Their hydrogen-bonding motifs and electron-rich characteristics make them promising candidates for material applications in carbon supplementing [14].

-Applications

-Photocatalysis: Carbon nitride is used in photocatalysis, which involves the acceleration of a photoreaction in the presence of a catalyst

- Electrocatalysis: It is also used in electrocatalysis, which involves the acceleration of electrochemical reactions

-Organic Synthesis: Carbon nitride plays a role in organic synthesis, which involves the construction of organic molecules [14].

-Importance

-Organic Semiconductor: Carbon nitrides are known as organic semiconductors with a band gap of 2.7 eV1. This makes them suitable for various electronic applications

-Potential Material Applications: Due to its hydrogen-bonding motifs and electron-rich properties, carbon nitride is considered a potential candidate for material applications in carbon supplementation

-Features

- These compounds are being investigated as potential next-generation materials for incorporation in devices for energy conversion and storage, as well as for optoelectronic and catalysis applications

- Light Harvesting and Photocatalysis: Carbon nitride solid state compounds are emerging as important materials for energy and sustainability applications ranging from visible-UV light harvesting and photocatalysis.

-Types

-Beta carbon nitride (β-C_3N_4): This is a solid that is predicted to be harder than diamond

-Graphitic carbon nitride (g-C_3N_4): This type is known for its important catalytic and sensor properties. It has large, tuneable band gaps and efficient intercalation of salts, making it useful for various applications such as photocatalysts, decomposition of water to H_2 and O_2, and degradation of pollutants

1.7. Composite

When two or more materials that differ greatly from one another in their physical and chemical composition are combined, composite materials are produced. The interactions between the several components give the composite its unique characteristics. [15]

1.8. literature survey

Concern over harmful organic pollutants entering water is growing, necessitating the development of efficient and sustainable methods to stop medicines from doing so. Degradation of organic contaminants depends on photocatalysis. This has sparked interest in the numerous applications of nanostructured perovskite in different energy and environmental domains. The application of the one-pot citrate nitrate technique for SrNiO3 production in photocatalysis is the novel feature of this work. It was reported that [16] the sample was calcined at 450 ◦C and 900 ◦C for 5 h. Crystalline phase purity, morphology, surface area, pore size, and optical properties were investigated through X-ray diffraction (XRD), scanning electron microscopy (SEM), Brunauer–Emmett–Teller (BET), Barrett-Joyner-Halenda (BJH), Fourier transform infrared spectroscopy (FTIR), and diffuse reflectance spectroscopy (DRS). The prepared sample of SrNiO3 was used as a photocatalyst for the photodegradation of naproxen, one of the most common pharmaceutical compounds detected in

wastewater. The effects of catalyst dose, naproxen amount, and reaction kinetics were investigated. After 60 min of UV irradiation exposure, the photocatalytic removal efficiency was found to be optimal using 1 g/L of SrNiO3. In summary, perovskite SrNiO3 exhibited excellent physicochemical and mechanical stability after five cycles of reaction.

It was reported that [17] lactose and glucose were used as fuels to create $SrNiO_3$/NiO/$SrCO_3$ nanocomposites in an eco-friendly manner. The impacts of different fuel concentrations on $SrNiO_3$/NiO/$SrCO_3$ nanocomposites were examined from both a pure and morphological standpoint. The crystal structure, morphology, optical, magnetic, and surface characteristics of the produced nanoparticles were investigated using a variety of physiochemical techniques. These methods included vibrating sample magnetometers, Brunauer-Emmett-Tellers, energy-dispersive spectroscopy (EDS), Fourier-Transform Infrared Spectroscopy (FTIR), scanning electron microscopy, transmission electron microscopy, and X-ray diffract. The as-synthesised nanoparticles' band gap was found to be 2.5 eV, indicating that they might function as a photocatalyst in conditions similar to those of sunshine. Using EDTA, benzoic acid, and benzoquinone as scavengers, the mechanism of the photocatalyst was examined, and the photocatalytic activity of $SrNiO_3$/NiO/$SrCO_3$ nanocomposites was assessed against methyl orange (MO) and methyl violet (MV). The degradation of MO (20 ppm) and MV in 60 minutes was associated with the highest degradation (92%) and 84.8%, respectively, according to a comparison of photocatalytic activity in UV and sun-like light. The findings suggest that auto-combusted $SrNiO_3$/NiO/$SrCO_3$ nanocomposites could be a potential photocatalyst for the rapid breakdown of organic contaminants in the environment.

Chapter 2: Experimental

2. Experimental Work

2.1. Materials

All chemical reagents were analytical grade and were used without further purification. The precursors nickel (II) nitrate hexahydrate ($Ni(NO_3)_{2.}.6H_2O$), Strontium nitrate hexahydrate ($Sr(NO_3)_2.6H_2O$) and sodium dodecyl sulphate (SDS, 99%) indigo carmine (IC, 99%) dye, urea (99%) and citric acid (98%) all provided from Aldrich.

2.2. Synthesis of materials

2.2.1. Synthesis of pure g-C_3N_4

The g-C_3N_4 sample was created via thermal treatment. In a muffle furnace, a ceramic crucible containing 20 g of urea was heated to 550 ^oC (15 ^oC/min) for four hours. The yellow g-C_3N_4 product was ground into a powder and allowed to cool to room temperature prior to use.

2.2.2. Preparation of $SrNiO_3$

$SrNiO_3$ was formed by mixing definite amounts of $Ni(NO_3)_{2.}.6H_2O$), $Sr(NO_3)_2.6H_2O$) and citric acid in molar ratios 1: 1:1 in 50 ml distilled water. 0.05 g of SDS as template dissolved in 10 ml distilled water was added to solution of metal nitrates mixture. Then citric acid was added to the above mixture under stirring at 90 ^oC for 3 h until gel was formed. The obtained gel was dried at 120 oC for 1 h. the final product was produced after heating at 900 ^oC for 5 h. It is denoted as SrNi.

2.2.3. Synthesis of $SrNiO_3$ /g-C_3N_4

$SrNiO_3$/g-C_3N_4 nanocomposite were prepared in ratios of 1:1. 0.9 g of g-C_3N_4 was dispersed in 100 ml of mixture of (1:1) ethanol and water under ultrasonication for 30 min. 0.9 g $SrNiO_3$ was added to the previous solution under stirring 1h and ultrasonicated for 1 h. The product was then filtered, washed several times with water, and then dried at 70 degrees for 12 hours. It is denoted as SrNiCN.

2.3. Catalytic activity measurements

Indigo carmine (IC) photocatalytic degradation on the produced materials was measured in order to assess the catalytic activity. To 0.05 g of the photocatalyst, 50 ml of a 20 ppm Indigo carmine dye solution was applied. Prior to irradiation, the reaction

mixture was agitated for half an hour. A visible light source was provided by an 80 W Xe lamp irradiation system. A 1 ml sample of the solution was taken out at regular intervals and its Indigo carmine dye content was measured. A Shimadzu spectrophotometer was used to measure the absorbance of the Indigo carmine dye spectrophotometrically at 610 nm. The following relationship was used to assess the photocatalytic efficiency: [1-C/Co] x 100 is the photodegradation efficiency.

2.4. Characterization

The crystalline phases of each sample under study were determined by X-ray diffraction (XRD) using a JDX:8030 X-Ray, JEOL, which is made in Japan. The patterns were run using Cu-filtered CuKα radiation ($\lambda > 1.5418$Å) that was energized at 45 kV and 10 mA. At room temperature, the samples were tested between $2\theta = 10$ and 80o. A KBr pellet was used to record the materials' infrared spectra on a German-made Brucker-FTIR (Vector 22). Using $BaSO_4$ as a standard, UV-Vis diffuse reflectance spectra (DRS) were captured in the 200–800 nm range using a Shimadzu UV-Vis spectrophotometer (2600i UV-Vis, Japan). The transmission electron microscope (TEM, FEI Tecnai G20) was used to evaluate the shape of the catalyst's particles.

Chapter 3: Results and Discussion

3. Results and Discussion

3.1. X-ray diffraction (XRD)

The crystal size and structure were ascertained by x-ray diffraction (XRD) analysis, which also examined the impact of the doping process on the crystal structure. The prepared samples' diffraction patterns are displayed in Figure 1. The (100) and (002) diffraction planes, which are typical of graphitic carbon nitride materials, are responsible for the two typical peaks in the XRD patterns of g-C_3N_4 nanosheets at 2θ= 13.29^o and 27.57^o. The in-plane structural packing motif is associated with the (100) plane, while the interlayer stacking of aromatic components is associated with the (002) plane [18].

The obtained XRD pattern of the analyzed sample calcined at 900 ^{o}C for 5 hours, as shown in Fig. 1, shows distinct diffraction peaks at 2θ = 29.5◦, 32.52◦, 37.7◦, 41.62◦, 45.2◦, 46.24◦, 50.14◦, 56.53◦, 58.03◦, and 60.95◦ JCPDS card no. (00–033–1347) planes of $SrNiO_3$ hexagonal phase respectively. Other sharp peaks that are associated with NiO can be found in JCPDS card no. (99–101–3531) at 2θ = 36.57◦, 37.72◦, 43.63◦, 63.16◦. In addition to appearance of peak at 22.6°, 26.3°, and 34.08^o related to Orthorhombic $SrCO_3$ according to JCPDS card no. (96-900-8199) and peaks at 27.3°, 27.9°, and 34.9° related to (002), (101), (110) planes of tetragonal SrO according to JCPDS card no. (96-101-0115).

The XRD pattern of SrNiCN composite shows several diffractions peaks referring to the presence of the hexagonal phase of $SrNiO_3$ (JCPDS card no. [00–033–1347]). In addition to the presence of peaks related to NiO (JCPDS card no. [99–101–3531]) and g-C_3N_4 indicating of formation of NiO@$SrNiO_3$/CN nanocomposite.

The average crystallite sizes were calculated using Debye–Scherrer equation based on all observed peaks in each pattern [19]: $D_{XRD}= K\lambda/\beta\cos\theta$

Where K is a constant equal 0.9, λ is the wavelength of the Cu Kα radiation, β is the full-width at half-maxima of the diffraction peak in radiant. The crystallite sizes of g-C_3N_4, and SrNi/CN were found 7.6, and 18 nm.

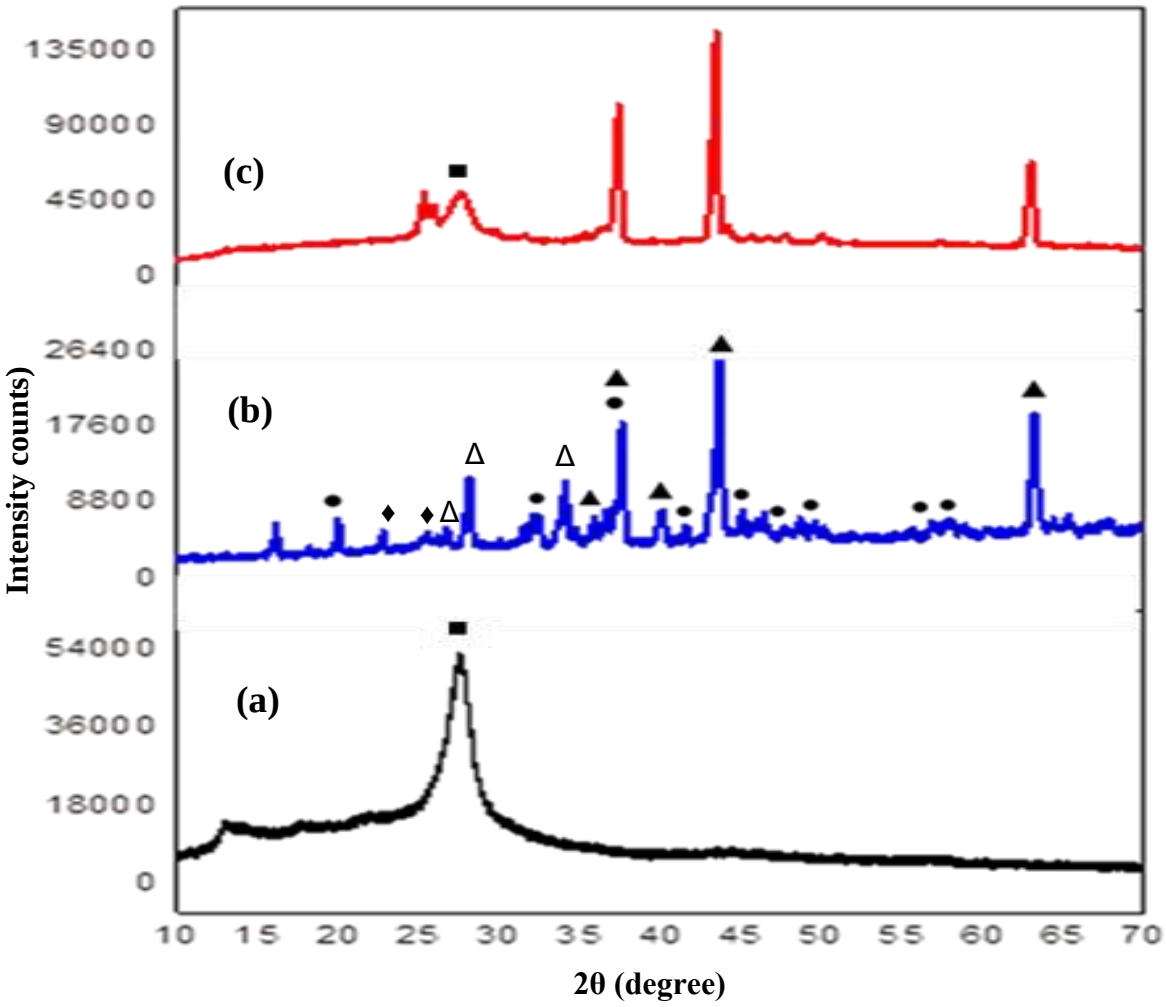

Fig. 1: XRD patterns of a) g-C_3N_4, b) $SrNiO_3$, and c) $SrNiO_3$/CN samples.

3.2. Fourier transforms infrared spectroscopy (FT-IR)

In Fig. 2, the FTIR analysis of strontium nickelate ($SrNiO_3$) nanocomposites made using the auto-combustion method provides crucial information about the material's structural properties and chemical makeup. Three distinct peaks in the spectrum can be identified, which identify important chemical bonds and possible contaminants. Peaks at 536, 758, and 856 cm^{-1} corresponded to Ni-O [20], Sr-O [21], and Sr-O [22-24], indicating that these crucial chemical bonds were present in the matter. Additionally, the peak at 3420 cm^{-1} represents the stretching vibrations of hydroxyl (OH) groups, which show that water molecules have adhered to the sample's surface. Further evidence of $SrCO_3$ as an impurity can be seen in peaks at 1462 cm^{-1}

that are ascribed to the bending vibrations of carbonate (CO_3^{2-}) ions. Peak appearance at 1624 cm^{-1} was associated with bending vibration of OH groups.

The SrNiCN composite's FTIR spectrum (Fig. 2) shows clear absorption peaks in range 473 cm^{-1} that correspond to Sr-O [21]. The bands at 1255, 1315, 1429, 1569, and 1644 cm^{-1} in this figure may be related to the typical stretching modes of CN heterocycles, whereas the absorption peaks at 810 cm^{-1} and 890 cm^{-1} are ascribed to the typical breathing mode of tri-s-triazine units and the deformation mode of N-H bonds, respectively [25, 26]. At the same time, the absorption band at 3197 cm^{-1} is produced by the stretching vibration of the N–H bond brought on by the uncondensed amino groups [27]. The findings show that g-C_3N_4 interacts with oxides.

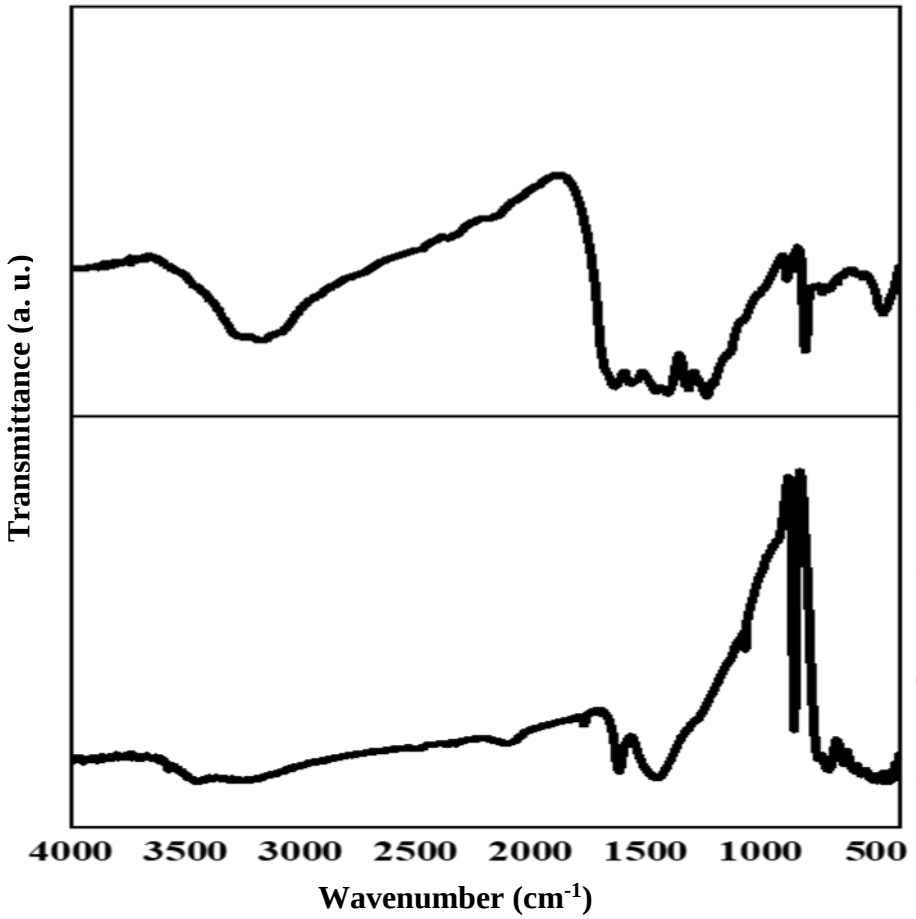

Fig. 2: FTIR spectra of g-C_3N_4 and SrNiCN.

3.3. TEM investigations

TEM images of SrNiCN nanocomposite were presented in Figure 3. The TEM images showed that two-dimensional porous structure constructed with curled and wrinkled nanosheets and platelets of the g-C_3N_4 (Fig. 3). the image shows also well dispersion of homogeneous nanowires of metal oxides with average length 10.4 nm on nanosheets of g-C_3N_4.

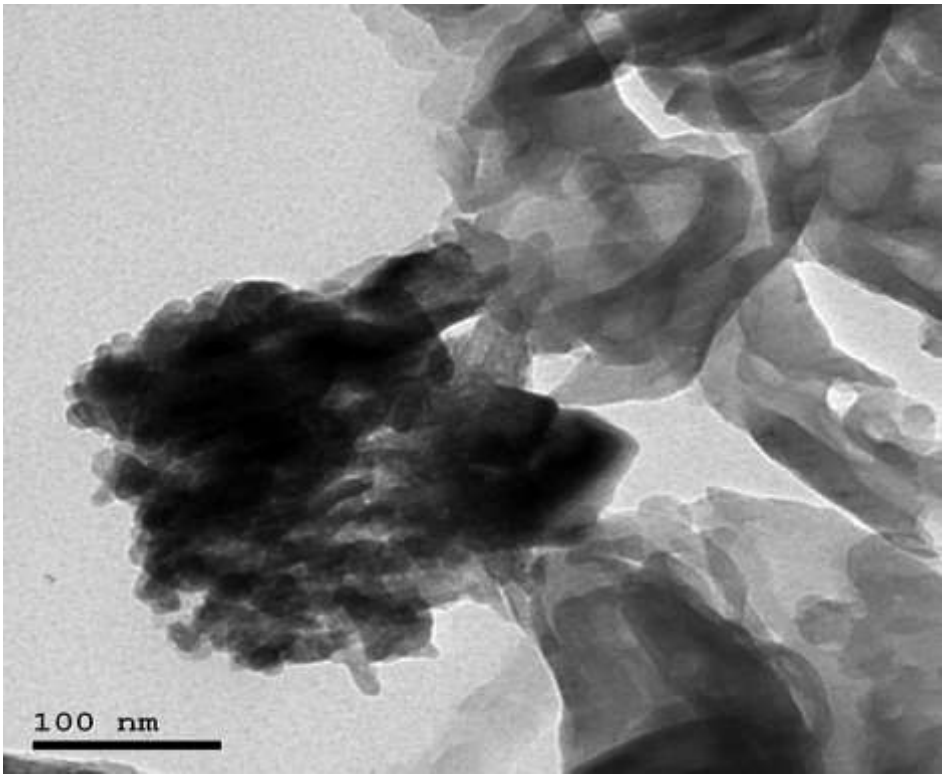

Fig. 3: TEM image of SrNiCN composite.

3.4. Optical properties

The optical characteristics of composite material are evaluated using UV-visible diffuse reflectance spectroscopy (UV-DRS), which works in the wavelength range of 200 to 800 nm, as shown in Figure 4a.

It is clear from the figure that the SrNiCN composite show noticeable absorption in the visible light region, which indicates the increased absorption of visible light of the composite.

The band gap energy of the samples can be roughly confirmed according to the plots in Fig. 4b, which is obtained via the Tuac equation $(\alpha hv)^{1/n} = B(hv- E_g)$

By calculating the power of n, a value of n=2 was revealed to propose an indirect permissible transition.

The energy gap values of samples can be determined from $(Ahv)^2$ vs. hν plot by linear extrapolation of the $(Ahv)^2$ to zero [28], as shown in Fig. 4b. The band gap energies of the SrNiCN composite was evaluated to be 2.96 eV (Fig. 4b).

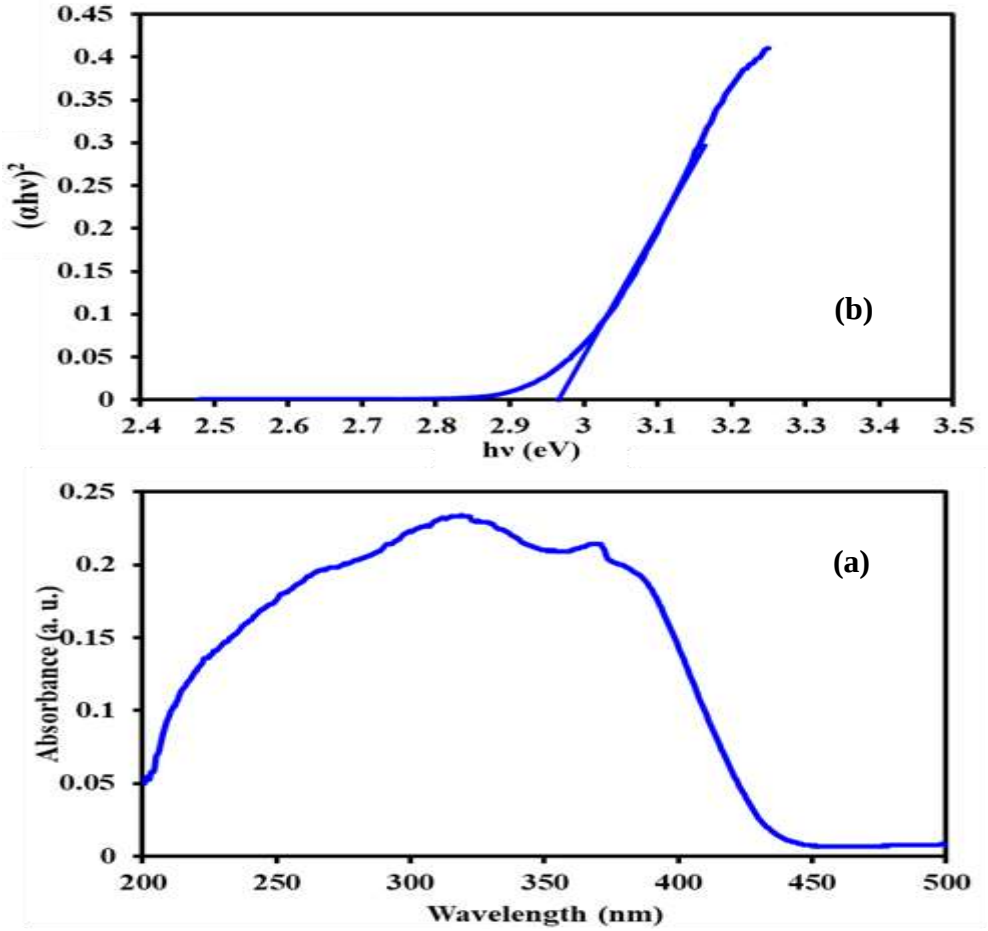

Fig. 4: The optical properties of SrNiCN sample a) UV-Visible absorbance, and b) Tauc`s curves for estimation of band gap.

3.5. Photocatalytic degradation

3.5.1. Photocatalytic activity studies

The photocatalytic degradation of IC dye on the SrNiCN nanocomposite surfaces, calculated at different pH values, is shown in Figure 5. The findings showed that when pH rises, degradation efficiency falls. While the adsorption rate sharply declines at a basic pH, the degradation is most pronounced at an acidic pH of 3. The catalyst's surface becomes positively charged as the pH of the solution drops, and the

electrostatic forces that pull the anionic IC dye molecules to the catalyst surface should encourage contact between them, increasing their effectiveness.

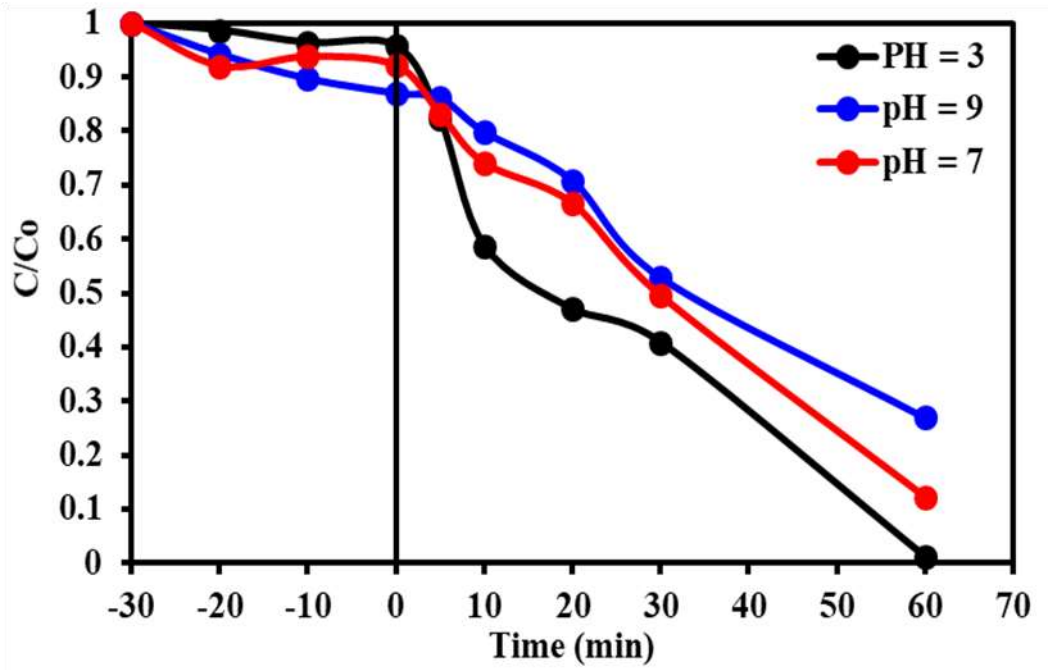

Fig. 5: Effect of pH on photo-degradation of indigo carmine dye on SrNiCN sample.

The photodegradation of IC dye on g-C_3N_4, $SrNiO_3$, and $SrNi_3$/g-C_3N_4 catalysts was given in Fig. 6. It was observed the catalytic degradation of pure catalysts (g-C_3N_4, $SrNiO_3$) were lower than that observed for $SrNiO_3$/g-C_3N_4 nanocomposite.

The catalytic degradation significantly increases to be 98.8% removal of dye at 60 min. It can be seen from Fig. 6a that the catalytic degradation rate under visible radiation increases in the following order as given in Table 1:

SrNi < CN < SrNiCN

These results show the synergetic effect of the three components on the catalytic activity. This may indicate that the photocatalytic method has improved the catalytic breakdown of the composite by reducing hole-electron recombination.

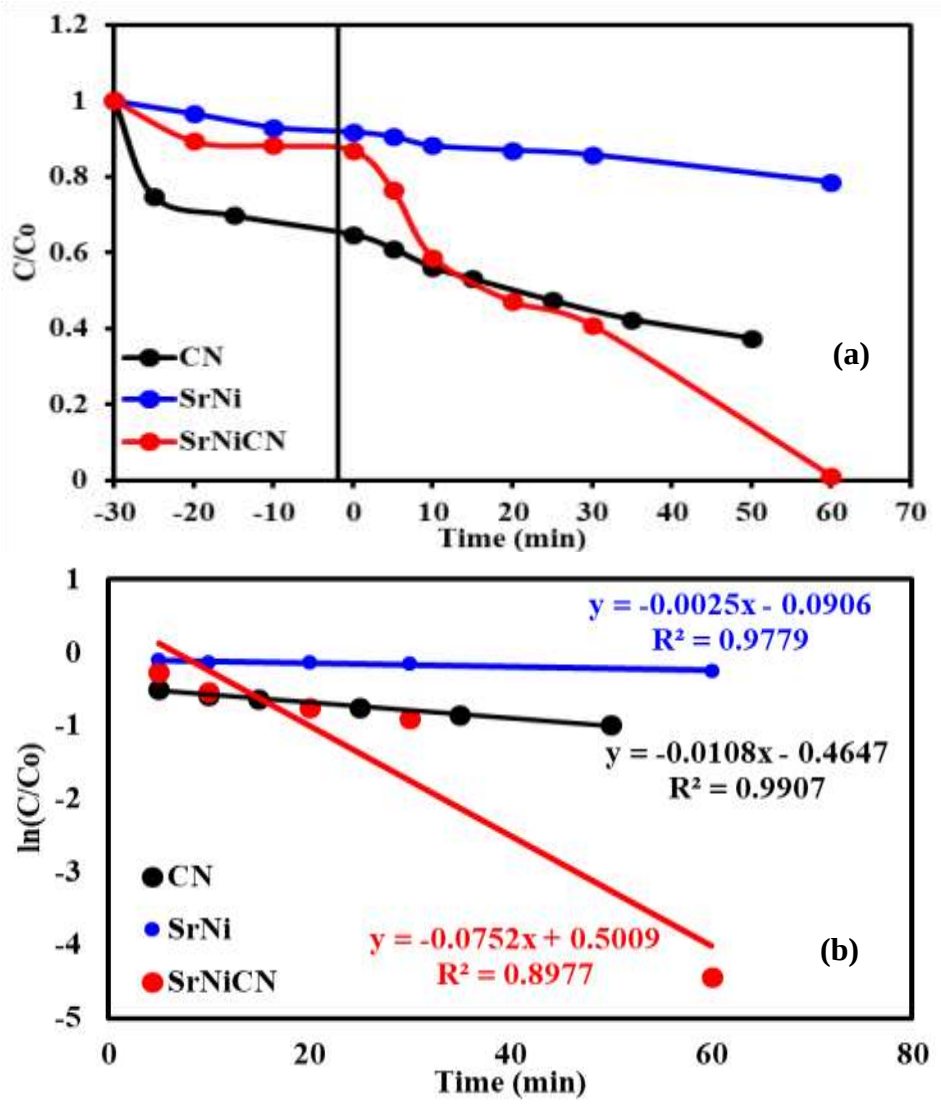

Fig. 6: a) Photodegradation of IC dye on all samples b) Kinetics of Photo-degradation of IC dye on different samples

3.5.2. Kinetic study:

Photocatalytic degradation of MG dye process was studied under visible illumination (Fig. 6b). According to many investigations, the impact of various experimental circumstances on the photocatalytic degradation rate of the majority of organic compounds was characterized using a pseudo-first order model (Eq. 1) [29–32].

$$-dC/dt = kap\ C \qquad (1)$$

Where k is the apparent rate constant and is affected by dyestuff concentration. Integration of that equation (with the same restriction of $C = C_o$ at $t = 0$) will lead to the expected relation:

$$\ln C = \ln C^o - Kt \qquad (2)$$

Plots of (lnC/Co) against time (t) for the dye degradation reactions under exposure to visible light are displayed in Fig. 6b. The apparent first-order rate constants (k) were calculated from the slopes of the plots, which displayed straight lines, and are shown in Table 1. It is obvious that k rises in the following order.

SrNi < CN < SrNiCN

Table 1: The photodegradation efficiencies and rate constant values of samples.

Sample	**Efficiency (%)**	**k (min^{-1})**
CN	62.2	0.011
SrNi	21.5	0.003
SrNiCN	100	0.075

4. Conclusion

Pure g-C_3N_4, $SrNiO_3$ and their nanocomposite were prepared by thermal and sol-gel method. XRD analysis shows the formation nanoparticles of all samples and formation of mixed phases of NiO, SrO and $SrNiO_3$. The obtained materials were tested for photocatalytic degradation of IC dye. The photocatalytic degradation efficiency was higher at pH =3 compared to other pH. The nanocomposite was found to have the highest photocatalytic activity with 100% degradation efficiency in 60 min with rate constant 0.075 min^{-1}.

,

References

[1] P. Kumari, M. Alam, W.A. Siddiqi, Sustain. Mater. Technol. 22 (2019) e00128.

[2] S. Shukla, R. Khan, A. Daverey, Environ. Technol. Innov. 24 (2021) 101924.

[3] S. Singh, V. Kumar, R. Romero, K. Sharma, J. Singh, Applications of nanoparticles in wastewater treatment, Nanobiotechnology Bioformulations 43 (2019) 395.

[4] R. Kalia, A. Chauhan, R. Verma, M. Sharma, K.M. Batoo, R. Kumar, S. Hussain,n S. Ghotekar, M.F. Ijaz, Phys. Status Solidi (a) 219 (2022) 2100539.

[5] M. Grzegorzek, K. Wartalska, B. Kaźmierczak, Intern. Commu. Heat Mass Transf. 143 (2023) 106674.

[6] S. Royer, D. Duprez, F. Can, X. Courtois, C. Batiot-Dupeyrat, S. Laassiri, H. Alamdari, Chem. Rev. 114 (2014) 10292.

[7] G. Mamba, P.J. Mafa, V. Muthuraj, A. Mashayekh-Salehi, S. Royer, T.I. T. Nkambule, S. Rtimi, Mater. Today Nano 18 (2022) 100184.

[8] Z.N. Garba, W. Zhou, M. Zhang, Z. Yuan, Chemosphere 244 (2020) 125474.

[9] R. Ji, J. Chen, T. Liu, X. Zhou, Y. Zhang, Chin. Chem. Lett. 33 (2022) 643.

[10] G.A. Samara, J. Phys.: Condens. Matter 15 (2003) R367.

[11] D. Kwon, I. Yang, Y. Sim, J.-M. Ha, J.C. Jung, Catal. Commun. 128 (2019), 105702.

[12] Y.A. Ivanova, E.F. Sutormina, N.A. Rudina, A.V. Nartova, L.A. Isupova, Catal. Commun. 117 (2018) 43.

[13] S. Park, H. Han, W. Yoon, J. Choi, Y. Kim, H. Kim, W.B. Kim, ACS Sustain. Chem. Eng. 8 (2020) 6564.

[14] M. Ismael, J. Alloys Compd. 846 (2020) 156446

[15] F. J. Heiligtag, M. Niederberger, Materials Today 16 (2013) 262.

[16] N. Aoun, H. Boucheloukh, K. Harrouche, B. Boughrara, T. Sehili, Inorg.Chem. Commun. 158 (2023) 111459.

[17] S. A. Ehsanizadeh, M. Goudarzi, E. A. Dawi, F. H. Alsultany, A. M. Aljeboree, M. Salavati-Niasari, Alexandria Eng. J. 108 (2024) 206

[18] X. Bai, L. Wang, R. Zong, Y. Zhu J. Phys. Chem. C 117 (2013) 9952.

[19] J. Mo, Q. Zhang, P. Xia, H. Chen, Z. Lu, H. Yang, Y. Chen, W. Xiao, Y. Wang, M. Liu, Solid State Commun. 356 (2022) 114961.

[20] M. Mogensen, S. Skaarup, Solid State Ion. 86–88 (1996) 1151.

[21] P. Balasubramanian, T.S.T. Balamurugan, S.M. Chen, T.W. Chen, J. Taiwan Inst. Chem. Eng. 81 (2017) 182.
[22] M.M. Rahman, M.M. Hussain, A.M. Asiri, RSC Adv. 6 (2016) 65338.
[23] M.M. Rahman, M.M. Hussain, A.M. Asiri, RSC Adv. 6 (2016) 65338.
[24] Z. T. Khodair, N. M. Ibrahim, T. J. Kadhim, A. M. Mohammad, Chem. Phys. Lett. 797 (2022) 139564.
[25] S.C. Yan, Z.S. Li, Z.G. Zou, Langmuir 25 (2009) 10397.
[26] F. Dong, Z. Zhao, T. Xiong, Z. Ni, W. Zhang, Y. Sun, W. Ho, ACS Appl. Mater. Interfaces 5 (2013)11392.
[27] T. Jayaraman, S. A. Raja, A. Priya, M. Jagannathan, M. Ashokkumar, New J Chem 39 (2015) 1367.
[28] P. R. Jubu, O. S. Obaseki, A. Nathan-Abutu, F.K. Yam, Y. Yusof, M. B. Ochang, Results in Optics 9 (2022) 100273
[29] X. L. Yan, T. Ohno, K. Nishijima, R. Abe, B. Ohtani, Chem. Phys. Lett., 429 (2006) 606.
[30] J. C. Yu, J. Yu, W. Ho, Z. Jiang and L. Zhang, Chem. Mater., 14 (2002) 3808.
[31] M. Anpo, M. Takeuchi, J. Catal., 216 (2003) 505.
[32] C. G. Wu, C. C. Chao, F. T. Kuo, Catal. Today., 97 (2004) 103.